Transactions of the **13th International Conference on Structural Mechanics in Reactor Technology** (SMiRT 13), Escola de Engenharia - Universidade Federal do Rio Grande do Sul, Porto Alegre, Brazil, August 13-18, 1995

Buckling strength of cylindrical shell subjected to thermal and mechanical loadings

Machida, H.[1], Kamishima, Y.[2], Kitade, S.[3], Nakashima, K.[3]
1) Advanced Reactor Technology Co., Ltd., Engineering Dept., Tokyo, Japan
2) Mitsubishi Heavy Industries, Ltd., Yokohama, Japan
3) Mitsubishi Heavy Industries, Ltd., Nagasaki, Japan

ABSTRACT : This paper describes the results of thermal buckling tests and elasto-plastic stress analysis for the cylinder subjected to axial temperature gradient and axial mechanical tension. The thermal buckling tests were carried out using a test model whose radius-to-thickness ratio was 200. The elasto-plastic stress analyses using the three-dimensional shell model have been carried out to investigate the effects of initial imperfection. The results of the tests have shown that the cylinder has structural integrity against thermal buckling. The effects of the initial imperfection on the stability of the cylinder have been found to be negligible.

1 INTRODUCTION

The primary coolant temperature of the Japanese demonstration fast breeder reactor, DFBR, is planned to be as high as 550℃ . Therefore a large axial temperature gradient appears in the vicinity of the sodium level of the reactor vessel.

A cylinder heated along its length does not buckle at any temperature because the destabilizing effect of the circumferential hoop compression near the thermal discontinuity is smaller than the stabilizing effect of the shape change of the cylinder as it is heated. However, when the axial temperature gradient is combined with axial mechanical tension, there is a possibility that it causes thermal buckling. This is because the axial tension restricts deformation due to the axial temperature gradient and forces to decrease the stabilizing effect of the shape change. At the 11th SMiRT conference Combescure and Brochard presented results of their study on thermal buckling of a thin walled cylinder subjected to combined loading of axial temperature gradient and axial mechanical tension [1]. Additionally, they presented a design diagram for a cylinder which has a radius-to-thickness ratio, R/t, of 500. It has been confirmed that there is no buckling behavior for thick wall cylinder whose R/t ranges 30 to 50 in a past Japanese study [2]. However, the buckling behavior has not been clarified for the reactor vessel of DFBR whose R/t is about 100.

To confirm the buckling behavior of the reactor vessel of DFBR, thermal buckling tests were carried out using a test model whose R/t was 200. The elasto-plastic stress analyses using the three-dimensional shell model have been carried out to investigate the effects of initial imperfection on buckling behavior. These results show that the reactor vessel of DFBR has structural integrity against thermal buckling.

2 THERMAL BUCKLING TEST

2.1 Test Model

The test model is shown in Fig. 1. It consists of a cylinder and a clamped flange attached at the top and the bottom ends of the cylinder to load axial tension. The cylinder is made of 304 stainless steel. Table 1 shows the results of the tensile strength test. The cylinder tested has a radius of 160mm, a thickness of 0.8mm and a height of 320mm. Its R/t is 200, and from the buckling strength point of view, it is on a sufficiently conservative side for the reactor vessel of DFBR. The initial imperfection of the general portion, except the vicinity of the welding line, is lower than its thickness.

2.2 Test Apparatus

Figure 2 shows the test apparatus. The test cylinder is placed on a fatigue test machine, and it is subjected to an axial tension load. The axial temperature gradient is given by injection heating and internal cooling water. A laser measuring instrument and a dial gauge are used for measuring circumferential and axial deformation of the cylinder, respectively. The temperature distribution is measured by CA-thermo-couples.

2.3 Test Condition

The test procedure is shown in Fig. 3. The maximum temperature gradient, which can be made using this test apparatus, is loaded to the cylinder. The temperature distribution is shown in Fig. 4. The circumferential membrane stress, σ_θ and the Tresca's equal stress, $\bar{\sigma}$, are as follows ;

$$\sigma_{\theta-m} = -30.4\ kgf/mm^2\ (\approx 2.0\sigma_y^H, \approx 1.0\sigma_y^C,\ \sigma_y^C = 31.1\ kgf/mm^2),$$

$$\bar{\sigma} = 62.0\ kgf/mm^2\ (\approx 4.2\ \sigma_y^H, \approx 2.0\ \sigma_y^C).$$

2.4 Test Results

Figure 5 shows the deformation of the cylinder after removing the loading every two thermal loading cycles. This deformation is measured at the level where the maximum compressed hoop stress appears. The uniform radial deformation increases every thermal loading cycle, but the buckling mode is not observed. Figure 6 shows the deformation of the cylinder at a high temperature compared with the deformation at the room temperature on condition that the cylinder is subjected to an axial loading. The buckling mode is not observed at the high temperature condition as well as at the room temperature.

3. ELASTO-PLASTIC STRESS ANALYSIS

3.1 Analytical Condition

Elasto-plastic stress analysis has been carried out using a three-dimensional shell model to confirm the effect of initial imperfection on thermal buckling behavior

subjected to an axial temperature distribution and an axial tension. A typical analytical model is shown in Fig. 7 and the material properties of the analytical model are shown in Table 2. The analytical model has a radius of 500mm, a height of 150mm and circumferential initial imperfection. The analytical parameters are the number of waves and the amplitude of circumferential initial imperfection, and the R/t of the cylinder. The initial imperfection is modeled as circumferential sinusoidal deformation. These analytical parameters and analytical cases are shown in Table 3. Figure 8 shows the typical loading condition; the axial mechanical loading is given first and then the axial thermal discontinuity is loaded.

3.2 Analytical Results

Figure 9 and 10 show typical cases of the deformation mode and the circumferential stress distribution, respectively. The maximum strain and stress appear at the bottom of the circumferential wave of the heated zone. Figure 11 shows the effect of the circumferential wave number on effective plastic strain at the portion where the maximum compression strain appears. When the number of waves is 3.0~4.0/30°, the effective strain increases above ~400℃ rapidly, and this increase is believed to cause buckling. However the behavior of effective strain does not change when the number of waves is less than 1.5/30°. Figure 12 shows the effect of the circumferential wave amplitude on the effective plastic strain. The amplitude of the initial imperfection does not effect when the amplitude of the initial imperfection is less than 0.25t practically. Figure 13 shows the effect on the effective plastic strain of the thickness of the cylinder. The increase of the strain does not appear when the R/t is less than 200. This result shows that the initial imperfection is not effective practically for the cylinder whose R/t is less than 200.

4 CONCLUSIONS

A thermal buckling test has been carried out under a severer than that of the reactor vessel of DFBR. When the cylinder, whose R/t is 200, subjected to an axial temperature gradient and an axial mechanical tension, the radial shrinkage is observed due to plastic deformation, but it is uniform and buckling mode has not been observed. This result shows that the reactor vessel of DFBR, whose R/t is 100, has structural integrity against thermal buckling sufficiently.

Elasto-plastic stress analyses using the three-dimensional shell model have been carried out to investigate the effects of initial imperfection on buckling behavior. The effects on the stability of the initial imperfection, which is assumed on DFBR's reactor vessel, have been found to be negligible when its R/t is less than 200.

REFERENCES

(1) A. Combescure, J. Brochard, Recent advances on thermal buckling new results obtained at C. E. A, 11th SMiRT volume E, p299-307.
(2) H. Ikeuchi et al, The effect of thernal rachetting on the buckling of a cylinder, 11th SMiRT volume E, p309-314.
(3) A. Combescure, Behabor of very thin cylindrical shells under moving axial gradient of temperature, 12th SMiRT volume E, p245-250.
(4) D. J. Johns et al, Buckling doe to thermal stress of cylindrical shells subjected to axial temperature distributions

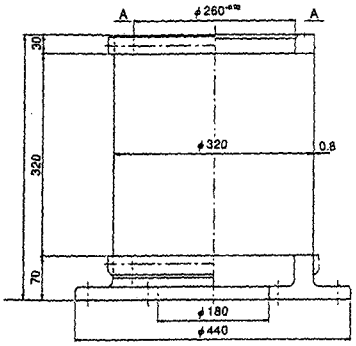

Fig. 1 Test model

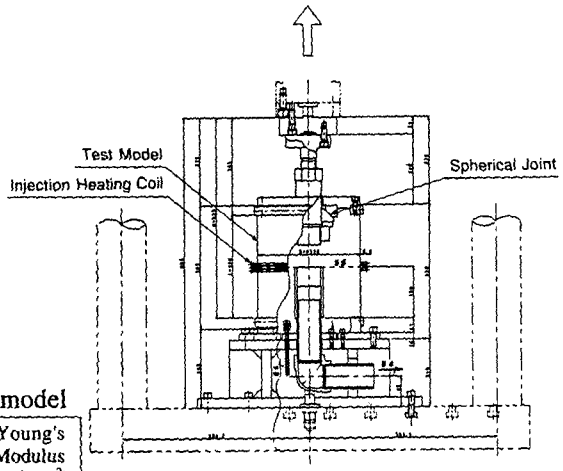

Fig. 2 Test apparatus

Table 1 Material properties of test model

Test Temp. (℃)	0.2% Yield Stress (kg/mm²)	Tensile Strength (kg/mm²)	Elongation (%)	Young's Modulus (kg/mm²)
R.T.	31.1	79.3	64.3	19900
300	19.5	52.5	31.7	17700
650	14.9	37.4	34.0	13500

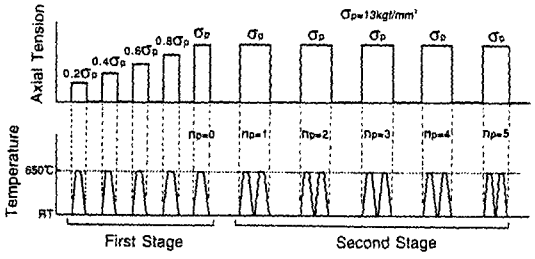

Fig. 3 Test procedure

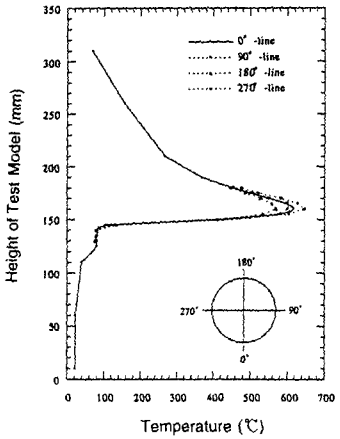

Fig. 4 Temperature distribution

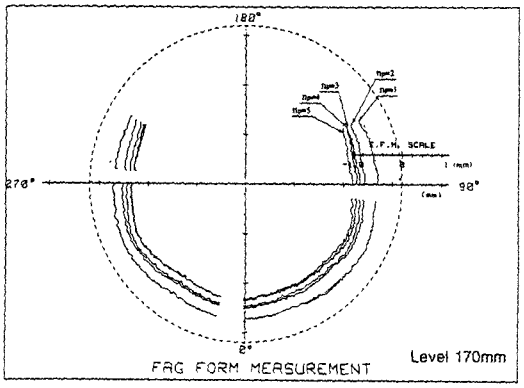

Fig. 5 Deformation of cylinder every two thermal loading cycles

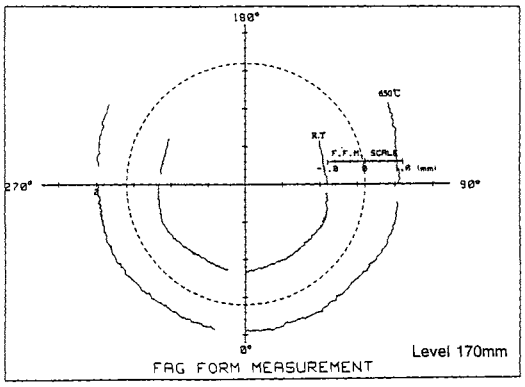

Fig. 6 Comparison of deformation at high and room temperature

Table 2 Material properties

Stress-strain Curve	Monotonic Curve
Young's Modulus	17200 (kg/mm^2)
Poisson's Ratio	0.3
Yield Stress	15.2 (kg/mm^2)
Coefficient of Linear Thermal Expansion	19.57 × 10^{-6} (1/℃)

Table 3 Analytical Cases

Analytical Case	R/t	Amplitude of Waves	Number of Waves
Reference	500	0.5t	3.5Waves / 30°
Case-11	500	0.5t	0.5Waves / 30°
Case-12	500	0.5t	1.5Waves / 30°
Case-13	500	0.5t	2.5Waves / 30°
Case-14	500	0.5t	3.0Waves / 30°
Case-15	500	0.5t	4.0Waves / 30°
Case-16	500	0.5t	5.0Waves / 30°
Case-21	500	0.1t	3.5Waves / 30°
Case-22	500	0.25t	3.5Waves / 30°
Case-23	500	1.0t	3.5Waves / 30°
Case-31	200	0.5t	3.5Waves / 30°
Case-32	100	0.5t	3.5Waves / 30°

$\sigma z / \sigma y = 0.4$: Const.

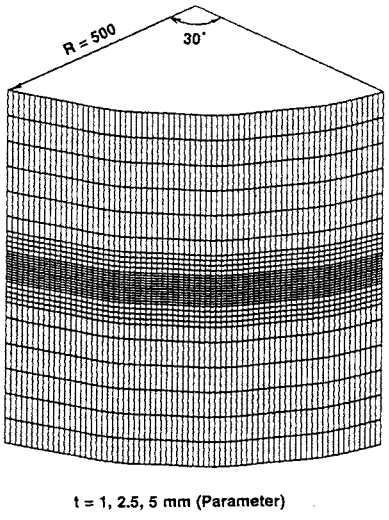

Fig. 7 Analytical model

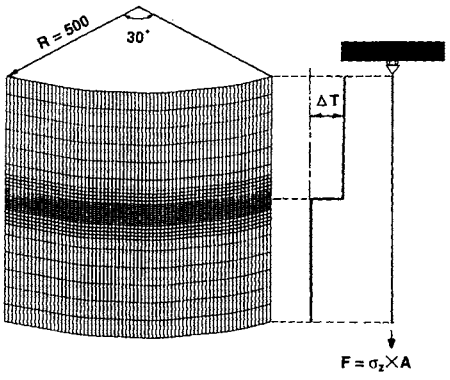

Fig. 8 Loading condition

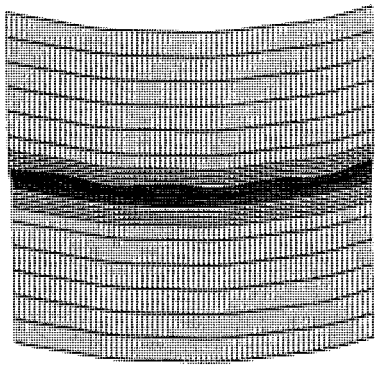

Fig. 9 Deformation mode
(Reference Case : 500℃)

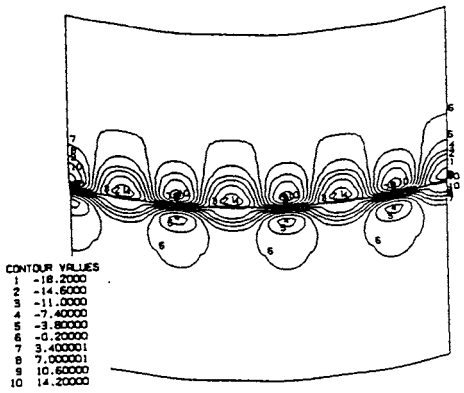

Fig. 10 Circumferential stress distribution
(Outer surface)

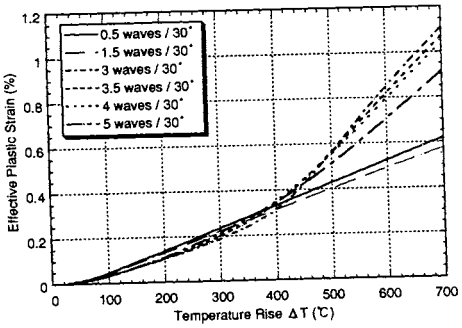

Fig. 11 Effect of initial imperfection
(circumferential wave number : N)

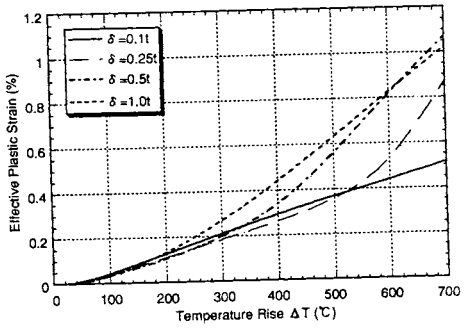

Fig. 12 Effect of initial imperfection
(circumferential wave amplitude : δ)

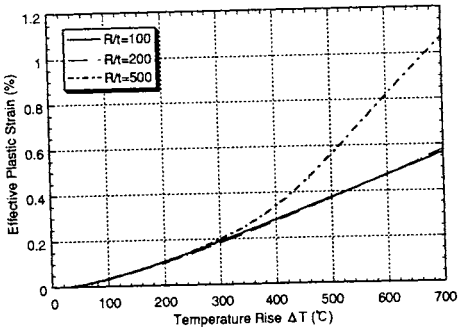

Fig. 13 Effect of initial imperfection (radius to thickness ratio : R/t)